Activation of Mast-Cell-Expressed Mas-Related G-Protein-Coupled Receptors Drives Non-histaminergic Itch

James Meixiong[1], **Michael Anderson**[1], **Nathachit Limjunyawong**[1], **Mark F. Sabbagh**[1], **Eric Hu**[1], **Madison R. Mack**[2,3], **Landon K. Oetjen**[2,3], **Fang Wang**[2,3], **Brian S. Kim**[2,3,4,5,*], and **Xinzhong Dong**[1,6,7,8,9,*]

[1]Solomon H. Snyder Department of Neuroscience, Johns Hopkins University School of Medicine, Baltimore, MD 21205, USA

[2]Center for the Study of Itch, Washington University School of Medicine, St. Louis, MO 63110, USA

[3]Division of Dermatology, Department of Medicine, Washington University School of Medicine, St. Louis, MO 63110, USA

[4]Department of Anesthesiology, Washington University School of Medicine, St. Louis, MO 63110, USA

[5]Department of Pathology and Immunology, Washington University School of Medicine, St. Louis, MO 63110, USA

[6]Department of Dermatology, Johns Hopkins University School of Medicine, Baltimore, MD 21205, USA

[7]Department of Neurosurgery, Johns Hopkins University School of Medicine, Baltimore, MD 21205, USA

[8]Howard Hughes Medical Institute

[9]Lead Contact

SUMMARY

Classical itch studies have focused on immunoglobulin E (IgE)-mediated mast cell activation and hista-mine release. Recently, members of the Mas-related G-protein-coupled receptor (Mrgpr) family have been identified as mast cell receptors, but their role in itch is unclear. Here, we report that mast cell activation via Mrgprb2 evoked non-histaminergic itch in mice independently of the IgE-Fc epsilon RI (FcεRI)-hista-mine axis. Compared with IgE-FcεRI stimulation, Mrgprb2 activation of mast cells was distinct in both released substances (histamine, serotonin, and tryptase) and the pattern of activated itch-sensory neurons. Mrgprb2 deficiency decreased itch in multiple preclinical models of allergic contact dermatitis (ACD), a pruritic inflammatory skin disorder, and both mast cell number and PAMP1–20 concentrations (agonist of the human Mrgprb2 homolog, MRGPRX2) were increased in human ACD skin. These findings suggest that this pathway may represent a therapeutic target for treating ACD and mast-cell-associated itch disorders in which antihistamines are ineffective.

In Brief

Classical itch studies have focused on IgE-mediated mast cell activation and histamine release. Meixiong et al. demonstrate that mast cell activation through the receptor Mrgprb2 contributes to non-histaminergic pruritus. Compared with IgE-FcεRI signaling, Mrgprb2-activated mast cells released more tryptase and excited a distinct itch-sensory neuron population. Mast-cell-associated Mrgprs may be therapeutic targets for itch associated with allergic contact dermatitis.

Graphical Abstract
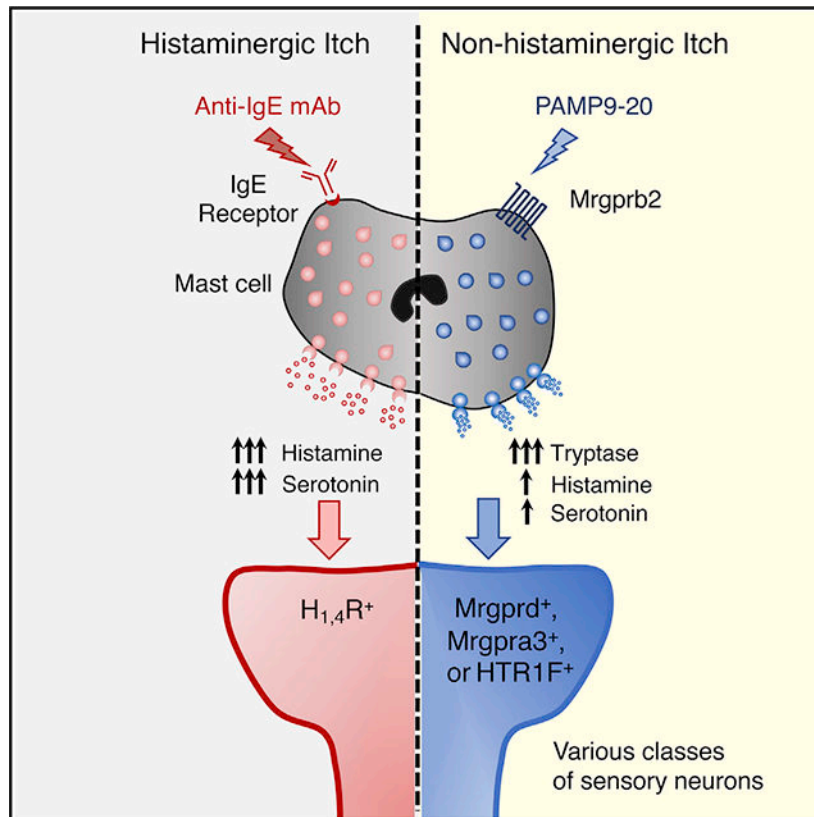
INTRODUCTION

Mast cells are the principle skin stores of numerous bioactive and immunomodulatory molecules such as chemokines, cytokines, histamine, serotonin, and tryptase (Metcalfe et al., 1997; Wernersson and Pejler, 2014). Upon activation, mast cells release compounds that can impact processes as varied as tissue remodeling, immune response, vascular tone, and nociception (Abraham and St John, 2010; Bischoff, 2007; Galli and Tsai, 2012; Meixiong and Dong, 2017; Ng, 2010). In the context of nociceptive itch (i.e., pruriception), mast cells are key cellular mediators via release of histamine, which activates receptors present on itch-sensory neurons of the dorsal root ganglia (DRG) (Shim and Oh, 2008).

Canonically, mast cell activation is understood to result from antigen binding to immunoglobulin E (IgE) antibody and cross-linking of the high-affinity IgE receptor, Fc epsilon RI (FcεRI). More recently, members of the Mas-related family of G-protein-coupled receptors (Mrgprs), Mrgprb2 in mice and MRGPRX2 in humans, have been identified as mast cell-expressed G-protein-coupled receptors (Kamohara et al., 2005; McNeil et al., 2015; Nothacker et al., 2005; Robas et al., 2003; Subramanian et al., 2011). Murine Mrgprb2 and human MRGPRX2 are activated by basic secretagogues, a class of positively charged molecules known to activate mast cells through a non-IgE mechanism (Galli and Tsai, 2012; Meixiong and Dong, 2017). Activation of either Mrgprb2 or MRGPRX2 results in mast cell degranulation that is both spatially and temporally distinct from FcεRI-mediated degranulation (Gaudenzio et al., 2016; McNeil et al., 2015). These observations provoke the hypothesis that mast cell Mrgpr pathways may promote itch in a unique fashion separate from classical IgE-mediated itch.

Despite their well-described roles in histaminergic itch, how mast cells interact with pruriceptive sensory nerves *in vivo* has not been investigated. Here, we report that activation of mast cells via Mrgprb2 induced itch distinct from classical IgE-FcεRI histaminergic itch. Compared to FcεRI activation, Mrgprb2 activation resulted in differential release of pruritogens. Using intravital Ca^{2+} imaging of sensory neurons, we showed that Mrgprb2-stimulation of mast cells, compared to IgE-FcεRI signaling, activated a distinct population of itch-sensory neurons. Histamine H_1 receptor (H_1R) blockade is not effective in treating numerous chronic itch disorders associated with mast cell activation such as allergic contact dermatitis (ACD) (Askenase et al., 1983; Dudeck et al., 2011; Erickson et al., 2018; Gimenez-Rivera et al., 2016; Grimbaldeston et al., 2007). In contrast, we demonstrated that Mrgprb2 was critical for itch in the setting of ACD and thus a possible target for therapeutic intervention.

RESULTS

Compared with FcεRI, Mrgprb2 Agonism Elicited Divergent, Non-histaminergic Itch Behavior and Differential Pruritogen Release

Although mast-cell-associated histaminergic itch is well studied, the precise role of Mrgpr signaling in mast cell itch is not known. Mrgprb2 (murine) and MRGPRX2 (human) are expressed in mast cells and not in other immune or neuronal cells (Flegel et al., 2015; McNeil et al., 2015; Motakis et al., 2014). We confirmed that Mrgprb2 expression was

specific to mast cells and not sensory neurons by crossing *Mrgprb2*-Cre mice expressing Cre recombinase under control of the *Mrgprb2* promoter with a tdTomato (tdT) reporter mouse line (*Mrgprb2*-Cre;tdT). *Mrgprb2*-Cre;tdT mice had no detectable tdT fluorescence in either DRG or spinal cord (Figures S1A–S1C). Concordantly, no *Mrgprb2* signal was detected in DRG or spinal cord using RT-PCR (Figure S1D). We employed pro-adrenomedullin peptide 9–20 (PAMP9–20) and compound 48/80, previously identified ligands of Mrgprb2 and MRGPRX2 (McNeil et al., 2015), to test whether activation of mast cells via Mrgprs was sufficient to induce itch *in vivo*. PAMP9–20 is a potent hypotensive peptide that is produced by a variety of cell types, including cells of the adrenal medulla and keratinocytes (Kapas et al., 2001; Kuwasako et al., 1997), and compound 48/80 is a canonical basic secretagogue activator of mast cells (Paton, 1951). Subcutaneous injection of either PAMP9–20 or compound 48/80 elicited itch in wild-type (WT) mice (Figures 1A and S2A) that was reduced in Mrgprb2-deficient (*Mrgprb2$^{-/-}$*) mice (Figures 1A and S2A). Neither substance elicited pain in the cheek model of behavior (i.e., wiping), indicating the specificity of acute Mrgprb2 activation for itch (Figures 1B, S2B, and S2C). To test whether pruritus resulted from mast cell activation, we injected PAMP9–20 into both cromolyn-treated and cKit^{W-sh} (SASH) mice. Cromolyn is a mast cell stabilizer that inhibits granule release, while SASH mice are c-Kit receptor-deficient animals that lack mast cells. Both cromolyn-treated animals and SASH mice displayed reduced PAMP9–20 itch compared to control animals (Figures 1C and 1D). *Mrgprb2$^{-/-}$* animals had intact mast cell itch responses to non-Mrgpr stimuli such as acute injection of anti-IgE, an antibody against mouse IgE, and repeated ovalbumin (OVA) exposure (Figures 1E and 1F). Anti-IgE directly crosslinks IgE and activates FcεRIα, while OVA sensitization results in a variety of OVA-specific immune responses including the generation of OVA-specific IgE (Reddy et al., 2012). Although the cellular expression of FcεRIα differs between mice and humans (de Andres et al., 1997), in mice, anti-IgE would be expected to specifically activate skin-resident mast cells (Figures S2D and S2E).

Both histamine (H$_1$ and H$_4$) and serotonin (5-HT$_2$ and 5-HT$_7$) receptor antagonism have been reported to be effective in controlling various forms of mast-cell-associated itch (Dunford et al., 2007; Katagiri et al., 2006; Morita et al., 2015; Shim and Oh, 2008; Yamaguchi et al., 1999). Indeed, cetirizine (H1R antagonist), JNJ7777120 (H4R antagonist), and the serotonin receptor antagonists ritanserin, mianserin, and cyproheptadine substantially reduced anti-IgE-associated itch (Figure 1G). In contrast, PAMP9–20-mediated itch was not significantly reduced by any tested antagonist (Figure 1H). Of note, the concentrations of ritanserin, mianserin, and cyproheptadine utilized (1 mg/kg) would inhibit not only serotonergic but also histaminergic receptors. Ondansetron, a 5-HT$_3$ antagonist, affected neither anti-IgE nor PAMP9–20 itch (Figures 1G and 1H). These data suggest that Mrgprb2 itch was not mediated by mast cell release of histamine and serotonin, indicating that Mrgprb2 activation may confer functions on skin-resident mast cells different from classical IgE-mediated activation. We stimulated murine peritoneal mast cells with PAMP9–20 and anti-IgE. At concentrations where mast cells were similarly activated, as determined by β-hexosaminidase release assay and Ca^{2+} imaging (Figures S2F and S2G), we detected differential release of well-known pruritogens. Compared with anti-IgE, PAMP9–20 resulted

in lower release of the monoamines histamine and serotonin and greater release of tryptase beta 2 (Figures 1I–1K).

Differential Mast Cell Activation Resulted in Divergent Sensory Neuron Excitation Profiles

In both rodents and humans, mast cells maintain a close anatomical relationship with sensory nerve fibers (Harvima et al., 2010). Such proximity supports a model whereby peptidergic sensory neurons can activate mast cells, and mast cells, in turn, can excite neurons via degranulation and release of effector molecules (Kleij and Bienenstock, 2005; van Diest et al., 2012). To explore how Mrgprb2 activation of mast cells might stimulate sensory nerves, we performed intravital Ca^{2+} imaging in Pirt-GCaMP6s mice after peripheral injection of Mrgprb2 agonists. Pirt-GCaMP6s mice express GCaMP6s, a genetically encoded fluorescent Ca^{2+} indicator, in >95% of sensory neurons (Kim et al., 2014) (Figures 2A and 2A′). Following injection of either PAMP9–20 (300 μM) or compound 48/80 (10 ng/mL) into the footpad of the ipsilateral hindpaw (part of the L4 dermatome), we observed robust activation of a subset of small-diameter sensory neurons in L4 DRG (Figures 2A–2C and S3A). PAMP9–20 and compound 48/80 activated a similar number of sensory neurons per trial, and both agonists activated significantly fewer neurons in *Mrgprb2*$^{-/-}$ mice (Figure 2B). In contrast, anti-IgE and direct activators of neurons, chloroquine (CQ), 5-HT, and β-alanine, excited an equivalent number of sensory neurons in both control and *Mrgprb2*$^{-/-}$ animals (Figures 2B, 2D, S3B, and S3C).

In vitro comparisons of Mrgprb2 agonism with IgE receptor activation have demonstrated that Mrgprb2 agonism triggers more rapid degranulation of smaller granules (Gaudenzio et al., 2016). Intravital Ca^{2+} imaging of mast cell-activated sensory neurons was consistent with this model. In comparison with anti-IgE-associated neurons, Ca^{2+} imaging traces of PAMP9–20-activated neurons displayed earlier excitation, increased numbers of Ca^{2+} signal peaks, and reduced total peakarea(amplitude3 duration) (Figures 2E–2G) (see STAR Methods for details). Neuronal excitation associated with either PAMP9–20 or anti-IgE was detected later than that associated with CQ, a direct activator of neuronal Mrgpra3 (Liu et al., 2009) (Figures 2E, S3D, and S3E).

Mrgprb2 and FcεRI Activation of Mast Cells Excited Distinct Populations of Itch-Sensory Neurons

Having established that differential activation of mast cells (IgE versus Mrgprb2) exhibited global differences in neuronal activation signatures, we were interested in examining the specific identity of activated sensory neurons. Based on divergent itch behavior (Figure 1), we hypothesized that differential activation of mast cells would excite separate classes of itch neurons *in vivo*. Single-cell RNA sequencing of mouse sensory neurons has determined three classes of itch neurons typified by expression of three G-protein-coupled receptors, *Mrgprd* (NP1), *Mrgpra3* (NP2), and *5ht1f* (NP3) (Usoskin et al., 2015) (Figure 3A). In order to identify itch neuron subtypes activated by mast cell agonism, we employed specific agonists for these receptors, b-alanine (Mrgprd), CQ (Mrgpra3), and 5-HT (5ht1f), to functionally identify neurons (Figures 3A and 3A′). Receptor expression is not strictly exclusive to each class of itch neuron. For example, a significant percentage (22%) of Mrgpra3-positive NP2 neurons express Mrgprd and thus would be expected to be activated

by both β-alanine and CQ (Usoskin et al., 2015). In the same imaging trial, repeat injections of the same activator should theoretically exhibit 100% overlap in excited neurons. However, in our trials, technical variability limited sensitivity. Of PAMP9–20-activated neurons, ~66% (50/76) were activated by a repeat injection of PAMP9–20. Subsequent percentage overlap data were thus normalized to this figure. Of all tested compounds, the two Mrgprb2 agonists, compound 48/80 and PAMP9–20, most consistently overlapped (Figure 3B). Mrgprb2-agonist-activated neurons exhibited broad overlap with neurons responsive to β-alanine (NP1), CQ (NP2), and 5-HT (NP3) and significantly less overlap with neurons sensitive to histamine and capsaicin (Figures 3C–3G). In contrast, anti-IgE-associated neurons overlapped significantly less with neuronal classes identified by β-alanine, CQ, and 5-HT and more with neurons responsive to histamine and capsaicin (Figures 3C–3G). Further, both cetirizine (H_1R antagonist) and JNJ7777120 (H_4R antagonist) preferentially decreased the number of anti-IgE-activated neurons compared to PAMP9–20-excited neurons (Figure 3H).

Mrgprb2 Promoted ACD-Associated Itch in Mice, and MRGPRX2 Agonists Were Elevated in Human ACD Skin

Given the role of Mrgprb2 in mediating non-histaminergic itch, we sought to investigate the relevance of Mrgprb2 in preclinical models of ACD, a chronic itch disorder associated with mast cell involvement (Askenase et al., 1983; Dudeck et al., 2011; Gimenez-Rivera et al., 2016; Grimbaldeston et al., 2007). ACD is a type IV hypersensitivity reaction that typically presents as an intensely pruritic, eczematous skin rash that is not amenable to antihistamine treatment (Kostner et al., 2017). In three separate models of ACD, squaric acetyl dibutyl acid (SADBE)- (Fu et al., 2014), oxazolone-, and dinitrochlorobenzene (DNCB)-treated mice exhibited significantly elevated itch compared to vehicle-treated controls. In all three models, $Mrgprb2^{-/-}$ animals scratched substantially less than WT mice (59% reduction in SADBE, 46% reduction in oxazolone, and 44% reduction in DNCB) (Figures 4A–4C). Compared to vehicle-treated skin, DNCB treatment resulted in an enrichment of immune cells as measured by $CD45^+$ cell numbers; however, DNCB-treated $Mrgprb2^{-/-}$ skin had significantly lower $CD45^+$ cell counts compared to WT skin (Figures 4D and 4G). Both WT and $Mrgprb2^{-/-}$ mice had similar ear skin thickness associated with ACD (Figure S4A). Further, $Mrgprb2^{-/-}$ mice were not protected from itch in the setting of either atopic dermatitis (MC903 or calcipotriol) or dry skin (acetone:ether [1:1] elicited), indicating that Mrgprb2 preferentially regulated ACD-associated itch (Li et al., 2006; Miyamoto et al., 2002) (Figures S4B and S4C).

Mast cells modulate ACD-associated inflammation (Askenase et al., 1983; Dudeck et al., 2011; Gimenez-Rivera et al., 2016; Grimbaldeston et al., 2007). Indeed, compared to healthy control skin, lesional skin from ACD had increased numbers of mast cells, as determined by avidin staining (Figures 4E and 4F). Multiple Mrgprb2 and MRGPRX2 agonists have been identified to be upregulated in ACD skin (El-Nour et al., 2006; Scholzen et al., 2001). Here, we found that expression of PAMP1–20, an Mrgprb2 and MRGPRX2 agonist, was similarly upregulated in ACD patient skin but undetectable in healthy control skin (Figures 4H and 4I). Adrenomedullin, the PAMP1–20 precursor, is produced by keratinocytes (Kapas et al., 2001). In support of this, we observed that anti-PAMP1–20 staining was specific to

epidermis (Figures 4H and 4I). A preabsorption control with PAMP1–20 peptide in hibited staining, supporting the specificity of the anti-serum used (Figures 4H″). Collectively, these findings support the hypothesis that mast cell-expressed Mrgpr signaling plays a role in the pathogenesis of ACD-associated itch in both mice and humans.

DISCUSSION

It is widely believed that mast cells, via the IgE-FcεRI-histamine axis, contribute to itch in a number of inflammatory skin disorders. However, histamine antagonists have been ineffective in treating many forms of allergic itch, suggesting that alternative mechanisms exist (Kamo et al., 2014; Liu et al., 2016; Usatine and Riojas, 2010). Here, we demonstrated that Mrgprb2 activation of mast cells, compared to classical IgE-mediated activation, promoted the differential release of pruritogens like tryptase beta 2 and evoked non-histaminergic itch. However, due to the complex composition of mast cell granules, Mrgprb2-associated non-histaminergic itch is likely caused by a number of pruritogens in addition to tryptase. Although largely histamine independent, a minor component of Mrgprb2-associated itch may be histaminergic, as antihistamines slightly reduced the number of sensory neurons activated by PAMP9–20. Conversely, IgE-FcεRI-associated itch displayed a non-histaminergic component that was resistant to histamine receptor antagonism. These findings suggest that despite clear divergence, some overlap exists between Mrgprb2- and FcεRI-mediated mast cell itch.

PAMP9–20-excited neurons most consistently overlapped with Mrgprd$^+$ itch neurons, while anti-IgE-associated neurons overlapped with histamine-sensitive neurons. In itch sensory neurons, H_1R expression and $Mrgprd$ expression do not overlap (Usoskin et al., 2015), indicating that PAMP9–20 and anti-IgE activated different populations of sensory neurons. One possible explanation for this difference in sensory neuron activation between PAMP9–20 and anti-IgE could be differential mast cell degranulation and release of compounds like tryptase beta 2. Tryptases cleave proteinase-activated receptors (PARs) present on itch-sensory neurons (Fu et al., 2014; Liu et al., 2011; Shimada et al., 2006). PARs such as $PAR4$ and $PAR2$ are preferentially expressed in Mrgprd$^+$ and 5ht1f$^+$ neurons, respectively (Usoskin et al., 2015).

Many chronic allergic itch conditions with mast cell involvement are refractory to histamine antagonists, indicating that alternative itch mechanisms exist (Kamo et al., 2014; Liu et al., 2016; Usatine and Riojas, 2010). ACD is one such condition with an enormous occupational health burden (Peiser et al., 2012). In ACD skin, multiple potential Mrgprb2 and MRGPRX2 agonists are upregulated. Indeed, we show that $Mrgprb2^{-/-}$ mice were protected from ACD-associated itch and that PAMP1–20 was enriched in lesional ACD patient skin. Despite a significant reduction in pruritus, $Mrgprb2^{-/-}$ animals had residual ACD itch, which could result from alternative mechanisms such as interleukin-33 (IL-33) activation of neuronal ST2 and T cell release of IL-31 (Liu et al., 2016; Takamori et al., 2018). Both mast cells and MRGPRX2 agonists are upregulated in atopic dermatitis and psoriasis (Nattkemper et al., 2018). However, $Mrgprb2^{-/-}$ animals did not exhibit reduced itch after topical MC903 treatment, a model of atopic dermatitis. Whether MRGPRX2 is an alternative mast-cell-associated target in pruritus of atopic dermatitis in humans remains to be defined.

Notwithstanding this, our murine studies suggest that Mrgprb2 played a preferential role in ACD compared to atopic dermatitis or dry skin.

Herein, we determined that activation of Mrgprb2 present on mast cells resulted in largely non-histaminergic itch. Our data showed that, compared with classical FcεRI signaling, Mrgprb2 agonism resulted in the release of different pruritogens from mast cells, resulting in the activation of a unique population of sensory neurons. Further, we found a major contribution of Mrgprb2 to ACD pruritus across a variety of murine models and enrichment of PAMP1–20, a Mrgprb2 and MRGPRX2 agonist, in human ACD skin. Collectively, our studies suggest that MRGPRX2 may represent a novel therapeutic target for treating ACD and other mast-cell-associated itch disorders in which antihistamines are ineffective.

STAR★METHODS

CONTACT FOR REAGENT AND RESOURCE SHARING

Further information and requests for resources and reagents should be directed to and will be fulfilled by the Lead Contact, Xinzhong Dong (xdong2@jhmi.edu).

EXPERIMENTAL MODEL AND SUBJECT DETAILS

Mice—Mice were housed 2–5 per cage with a 12-hour light/dark cycle and *ad libitum* access to rodent chow and water. Behavior assessments were performed during the light phase. All experimental protocols were approved by the Animal Care and Use Committee at the Johns Hopkins University School of Medicine (Protocol Number: MO16M40). All mice used for this study were born and bred within Hopkins Miller Research Building Animal facility and weaned at 3–3.5 weeks of age. Mice used for experiments were 1.5–3 months old males and females (20 – 30 g) on the C57BL/6 background. Mrgprb2 −/− and Mrgprb2-Cre animals were generated as previously described (McNeil et al., 2015). Pirt-cre animals were generated as previously described via homologous recombination (Kim et al., 2016). Rosa26-LoxP-STOP-LoxP (lsl)-GCaMP6s and Rosa26-LoxP-STOP-LoxP (lsl)-tdTomato mice were purchased from Jackson Labs. Pirt-cre; Rosa26-lsl-GCaMP6s mice were obtained by crossing Pirt-cre animals with lsl-GCaMP6s animals. Mrgprb2-cre; Rosa26-lsl-tdTomato mice were obtained by crossing Mrgprb2-cre animals with lsl-tdTomato animals. cKit^{W-sh} (SASH) mice were obtained from Jackson Labs.

Human Skin Sample Collection—De-identified human skin tissues were obtained under IRB-exempt protocols through the Division of Dermatology at Washington University School of Medicine and the Skin Biology and Diseases Resource-based Center at the Perelman School of Medicine at the University of Pennsylvania. Allergic contact dermatitis lesional skin was obtained from eleven patients aged 17 – 89. Eight patients were female, and three patients were male. Healthy control skin was taken from eight patients aged 29 – 47. All healthy skin was collected from female patients. Besides allergic contact dermatitis where indicated, all patients were otherwise healthy. Skin tissue sections from were obtained from biopsy specimens that were fixed in 10% neutral buffered formalin and embedded in paraffin.

METHOD DETAILS

Peritoneal Mast Cell Primary Culture—Peritoneal mast cells were isolated from adult male and female mice as previously described (McNeil et al., 2015). A peritoneal lavage was performed. Mast cells were isolated from the cellular contents using a 70% percoll gradient, spun at 500 r*cf.* for 20 minutes at 4°C. Cell pellets were washed, and mast cells were plated onto fibronectin-coated coverslips or cell culture wells. Mast cell purity among isolated cells was assessed with toluidine blue staining. > 95% of isolated cells were stained by toluidine blue and thus determined to be mast cells. Isolated cells were cultured with mouse stem cell factor (SCF) (25 ng/mL) for two hours at 37°C before further experimentation.

Immunofluorescence Imaging of Mrgprb2-Cre; tdT Animals—
Immunofluorescence imaging was performed as previously described (Han et al., 2013). Briefly, *Mrgprb2*-Cre; tdT animals were anesthesized with chloral hydrate before fixation with 4% paraformaldehyde. After fixation, primary tissues of interest, dorsal root ganglia, spinal cord, and skin were dissected, post-fixed in 4% PFA for 1 hr at RT, before incubation with 20% sucrose then 30% sucrose. Tissues were embedded in OCT and sectioned on a cryotome. Sections were dehydrated and stained with IB4–488 for 1 hour at RT before imaging on a Zeiss LSM700 confocal microscope.

RT-PCR—RNA was purified from dissected DRG, spinal cord, and approximated 1×10^5 peritoneal mast cells with QIAGEN RNEasy Micro columns, according to the manufacturer's suggestions. RNA was treated for 20 minutes with DNase I (New England BioLabs) before being used to generate first strand cDNA using a SuperScript III kit (Invitrogen) according to the manufacturer's instructions. A negative control reaction was included where SuperScript III reverse transcriptase was replaced by water. 25 μL PCR reactions were run with 12.5 μL RedTaq ReadyMix (Sigma), 0.5 μL DMSO, 0.25 μL each of 50 μM gene-specific forward and reverse primers, 10 μL water, and 2 μL mixture from either cDNA or negative control synthesis reactions. PCR reaction included a 4 minute initial step at 95°C, 30 s annealing at 62°C, 40 s extension at 72°C, and 25 s at 95°C (with the last three steps repeated 39 times), and a final 4 minute step at 72°C. Primers for *MrgprB2* were forward gtcacagaccagtttaacacttcc, reverse cagccatagccaggttgagaa.

Behavioral Tests—All applicable behavioral tests were performed and analyzed with the experimenter blind to genotype. For all studies, male and female mice age 1.5 −3 months were used. No sex- or ag-based differences were found for any analysis. Experiments were designed in a blocked fashion with regards to genotype, sex, and age of mice. Itch behavior experiments were performed between 8 a.m. and 12 p.m. The day prior to experimentation, animals were habituated in the test chamber for 30 minutes underdoing a series of three mock injections. On the day of the experiment, animals were allowed to acclimatize to the test chamber for 10 minutes prior to injection. Pruritic compounds were subcutaneously injected into the nape of the neck or cheek, and scratching behavior was observed for 30 minutes. For the nape, we injected compounds in a 50 μL volume. For cheek, 10 μL was used. A bout of scratching was defined as a hindpaw directed continuous scratching movement at the injection site. In the cheek injection model, a wipe was defined as a single forepaw stroking the site of the injection. Use of both forepaws was classified as grooming

behavior and not counted. Scratching behavior was quantified by counting the number of scratching bouts during the 30-min observation period. Wiping was quantified during a 30-minute observation period. All pharmacologic antagonists were given intraperitoneally 30 minutes prior to injection of test compound. Mast cell stabilizer, cromolyn, 25 mg/kg. H1R block, 30 mg/kg of cetirizine HCl (pH 7.4); H4R block, 40 mg/kg of JNJ7777120; ritanserin block, 1 mg/kg ritanserin; mianserin block, 1 mg/kg mianserin; cyproheptadine block, 1 mg/kg cyprohepta-dine; ondansetron block, 1 mg/kg ondansetron.

Peritoneal Mast Cell Isolation, *In Vitro* Experimentation, and Detection of Released Contents, Histamine, and Tryptase Beta 2—For calcium imaging experiments, mast cells were incubated with the calcium dye Fluo-4 for 30 minutes before imaging. For all mast cell granule release assays, β-hexosaminidase, histamine, and Tryptase Beta 2, $1\times10^4 – 5\times10^4$ mast cells were incubated with test compound for 30 minutes before supernatant was collected. All assay results were normalized according to cell number. For, β-hexosaminidase release, lysate was collected after addition of 0.5% Triton X-100. Both supernatant and lysate were incubated with 1mM 4-Nitrophenyl N-acetyl-b-D-glucosaminide (PNAG) solution for 1.5 hr at 37°C. 10mM Glycine, pH 10 was added to stop the reaction, and absorbance at 405nm was read on a Flexstation 3 (Molecular Devices). Histamine was detected with an ELISA kit from Enzo Lifesciences according to manufacturer's instructions. Tryptase beta 2 was detected with an ELISA kit from Cusa Bio according to manufacturer's instructions.

DRG Exposure Surgery for *In Vivo* Imaging of the Whole L4 DRG—DRG exposure surgery was performed as previously described (Kim et al., 2014). Throughout the surgery, mice were kept on a heating pad (DC temperature controller, FHC) to maintain body temperature at 37°C ± 0.5°C as monitored by rectal probe. Mice were anesthetized by i.p. injection of sodium pentobarbital (40 mg/kg) and their backs were shaved and disinfected. Ophthalmic ointment (Lacrilube; Allergen Pharmaceuticals) was then applied. An approximately 2-cm midline incision was made at the lower part of the lumbar enlargement and 0.1 mL of 1% lidocaine was injected into the paravertebral muscles before they were dissected away to expose L3–L5 vertebrae. Using rongeurs, the surface aspect of the L4 DRG transverse process was removed and the underlying DRG was exposed. Bleeding was stopped using styptic cotton.

***In Vivo* DRG Calcium Imaging**—*In vivo* imaging of whole L4 DRG was performed for 1–3 hours immediately following surgery. Images were acquired using a laser-scanning confocal microscope (Leica LSI microscope) equipped with a 53 0.5 NA macro dry objective and fast EM-CCD camera. Live images were acquired at 8 to 10 frames in frame-scan mode per 7–8 s, at depths of 0 to 70 mm below the dura with the DRG in the focal plane. Throughout imaging, body temperature was maintained at 37°C ± 0.5°C with a heating pad and rectal temperature monitoring. Anesthesia was maintained with 2% isofluorane and pure oxygen delivered through nosecone. Mice were laid abdomen-down on a custom-designed microscope stage. The spinal column was secured at two sites using clamps. Imaging was monitored during the activation of DRG neuron cell bodies by

peripheral stimuli (5 μL of the stated concentration of either mast cell or neuronal activators) delivered via Hamilton syringe.

***In Vivo* Calcium Imaging Data Analysis**—For imaging data analysis, raw image stacks were collected, deconvoluted, and imported into ImageJ (NIH). Optical planes from sequential time points were re-aligned and motion corrected using the stackreg rigid-body cross-correlation-based image alignment plugin. The number of counted activated neurons between different mice and different DRG imaging periods was normalized to the total number of neurons present in the DRG. The total number was counted using the thresholding function in ImageJ software from a high-quality, Z stack image of DRG at baseline. The size of activated neurons was calculated using the area function in ImageJ.

Calcium signaling amplitudes were normalized F_t/F_0 as a function of time. F_0 was defined as the average pixel intensity during the first two to six frames of each imaging experiment. Changes in fluorescence were measured from all neurons that displayed a change from baseline and selected for further analysis. In subsequent analysis, neurons that displayed < $0.2 F_0$ change in baseline, were only active during the injection period, and displayed a > 0.2 F_0 change during either the baseline or the saline imaging periods were excluded from analysis. The peak area was measured using the area under the curve (AUC) functionality in GraphPad PRISM. Signal peaks were defined as a > $0.2F_0$ increase over baseline followed by either a return to baseline ± 10% or normalization of signal by > $0.2F_0$. Shoulder peaks were defined as those peaks that occur before both a return from peak to baseline ± 10% F_0 and before normalization of signal by > $0.2F_0$ and were excluded from analysis. There is significant activation associated with injection into the paw. In determining whether a neuron was activated within an imaging window, the neuron, represented by its designated region of interest (ROI) needed to exhibit multiple peaks of > $0.2F_0$ from baseline outside of the first minute after injection. All putative responding cells and counted peaks included in analysis were verified visually using the raw imaging data and individual neuron calcium traces. The average F_t/F_0 values for specific ROIs were tested for statistical significance by repeated-measures ANOVA, followed by Mann-Whitney statistics. Fiji (NIH), LIF (Leica), and PRISM software were used to analyze and plot Ca^{2+} imaging data.

Flow Cytometry—For FcERIa[+] cell isolation. Cheek tissues were shaved and digested with 0.25 mg/mL Liberase TL (Roche) in DMEM at 37 C and 5% CO_2 for 90 minutes prior to homogenization through a 100 mm cell strainer in DMEM with 5% FBS. Single cell suspensions were stained with ZombieUV viability dye per manufacturer's instructions (Biolegend) followed by primary antibodies on ice for 30 minutes. Primary antibodies (Biolegend unless otherwise specified) were: CD45 PE, CD11b BV510, Lin PerCP/Cy5.5, c-Kit BV605, FcERIa FITC (eBioscience), IgE FITC (eBioscience). Lineage (Lin) cocktail included (eBioscience): CD3e, CD5, CD19, CD11c, NK1.1.

For CD45^{+} cell isolation from allergic contact dermatitis skin. Mice were sensitized with 2% DNCB on their abdomen. Five days later, 1% DNCB was used to elicit allergic contact dermatitis on the ear. After 24 hours, ears were excised using a 6mm biopsy punch, cut into small pieces and placed in RPMI1640 media containing 1.25 mg/ml Dispase II, 2 mg/ml Collagenase II and 2 mg/ml Collagenase IV. Tissues were incubated at 37°C for

approximately 75mins. The digested ear tissues were passed through a 70 mm cell strainer, pelleted and washed in PBS. Cells were stained with Aqua Live/Dead viability dye according the manufacturer's manual to exclude non-viable cells. Then cells were blocked for non-specific binding in buffer containing anti-mouse CD16/CD32 Fc blocker for 10 minutes prior to staining with the CD45-FITC. Data were acquired with a CytoFLEX LX (Beckman Coulter), and the analysis was performed using FlowJo v10 software (TreeStar).

Ovalbumin and Allergic Contact Dermatitis Itch Models—For ovalbumin associated itch, we first sensitized animals by injecting 50 mg of ovalbumin in phosphate-buffered saline (PBS) with 2 mg of aluminum hydroxide i.p. 10 days later, animals were re-injected i.p. with 20 mg of ovalbumin in PBS containing 2 mg of aluminum hydroxide. After one week, 50 μg of ovalbumin in saline was administer and scratching behavior was quantified. Contact dermatitis model was performed by first shaving the abdomens of animals the day prior to experimentation. Shaved abdomens were treated with 40 μL of either 3% DNCB, SADBE, or Oxazolone dissolved in acetone: olive oil (4:1 v/v) QD for three days. After four days, the nape of the neck of animals were shaved. The next day, 1% DNCB, SADBE, or Oxazolone dissolved in acetone: olive oil (4:1 v/v) was applied to shaved skin QD for three days. The next day, animals were habituated by being placed in the test chamber for 1 hour. The following day, behavior was assessed, and skin samples were collected. For skin thickness measurements, animals were sensitized with 100 μL of either 3% DNCB, SADBE, or Oxazolone dissolved in acetone: olive oil (4:1 v/v) on shaved abdomen. Five days later, 10 μL of respective agent was applied to each side of the right ear. At the same time, 10 μL of vehicle was applied to each side of the left ear. 24 hours later, ear thickness of both right and left ears was assessed with Mitutoyo digimatic calibrator.

Immunohistochemistry with Paraffin-Embedded Sections—Paraffin embedded skin samples were stored until needed at 4°C. Slides were deparaffinized with 2 changes of xylene for 5 minutes and 3 minutes changes of the following solutions: 100% ethanol, 95% ethanol, 70% ethanol, and 50% ethanol before rinsing with distilled water. Antigen retrieval was done by heating the slides to boiling in Tris-EDTA buffer (10mM Tris, 1mM EDTA, 0.05% Tween20, pH 9) placed within a pressure cooker (Nordic ware). Sections were permeabilized with PBST, blocked with 10% normal goat serum for 1 hour at room temperature, and then incubated with primary antibody (1:500 for PAMP antiserum; 1:500 for avidin-FITC) diluted in 10% normal goat serum overnight at 4°C. For preabsorption control, 1:500 diluted anti-serum was incubated with 100mM PAMP1–20 peptide for 1 hr at room temperature before applied like primary antibody. The next morning, slides were rinsed three times with TBS 0.025% Triton before application of secondary antibody (1:500) diluted in 10% goat serum. Slides were incubated for 1 hour at room temperature and washed three times with TBS 0.025% Triton before being mounted with anti-Dapi medium (Vector Labs). Sections were imaged using a Zeiss LSM700 confocal microscope and images were analyzed with ImageJ.

QUANTIFICATION AND STATISTICAL ANALYSIS

Group data were expressed as mean ± standard error of the mean unless otherwise noted. Two-tailed unpaired Student's t tests and two-way ANOVA tests were used to determine

significance in statistical comparisons; differences were considered significant at p < 0.05. Statistical power analysis was used to justify sample size for all behavior experiments. Variance for all presented treatment groups was similar as determined by F test. No samples or animals subjected to successful procedures and/or treatments were excluded from analysis. All behavior experiments were designed in a blocked manner with consideration for both genotype and treatment. Statistical details for each experiment can be found in figure legends.

Supplementary Material

Refer to Web version on PubMed Central for supplementary material.

ACKNOWLEDGMENTS

REFERENCES

Abraham SN, and St John AL (2010). Mast cell-orchestrated immunity to pathogens. Nat. Rev. Immunol 10, 440–452. [PubMed: 20498670]

Askenase PW, Van Loveren H, Kraeuter-Kops S, Ron Y, Meade R, Theoharides TC, Nordlund JJ, Scovern H, Gerhson MD, and Ptak W (1983). Defective elicitation of delayed-type hypersensitivity in W/Wv and Sl/SId mast cell-deficient mice. J. Immunol 131, 2687–2694. [PubMed: 6605986]

Bischoff SC (2007). Role of mast cells in allergic and non-allergic immune responses: comparison of human and murine data. Nat. Rev. Immunol 7, 93–104. [PubMed: 17259966]

de Andres B, Rakasz E, Hagen M, McCormik ML, Mueller AL, Elliot D, Metwali A, Sandor M, Britigan BE, Weinstock JV, and Lynch RG (1997). Lack of Fc-epsilon receptors on murine eosinophils: implications for the functional significance of elevated IgE and eosinophils in parasitic infections. Blood 89, 3826–3836. [PubMed: 9160690]

Dudeck A, Dudeck J, Scholten J, Petzold A, Surianarayanan S, Köhler A, Peschke K, Vöhringer D, Waskow C, Krieg T, et al. (2011). Mast cells are key promoters of contact allergy that mediate the adjuvant effects of hap-tens. Immunity 34, 973–984. [PubMed: 21703544]

Dunford PJ, Williams KN, Desai PJ, Karlsson L, McQueen D, and Thurmond RL (2007). Histamine H4 receptor antagonists are superior to traditional antihistamines in the attenuation of experimental pruritus. J. Allergy Clin. Immunol 119, 176–183. [PubMed: 17208599]

El-Nour H, Lundeberg L, Al-Tawil R, Granlund A, Lonne-Rahm SB, and Nordlind K (2006). Upregulation of the axonal growth and the expression of substance P and its NK1 receptor in human allergic contact dermatitis. Immunopharmacol. Immunotoxicol 28, 621–631. [PubMed: 17190739]

Erickson S, Nahmias Z, Rosman IS, and Kim BS (2018). Immunomodulating agents as antipruritics. Dermatol. Clin 36, 325–334. [PubMed: 29929604]

Flegel C, Schöbel N, Altmüller J, Becker C, Tannapfel A, Hatt H, and Gisselmann G (2015). RNA-seq analysis of human trigeminal and dorsal root ganglia with a focus on chemoreceptors. PLoS ONE 10, e0128951. [PubMed: 26070209]

Fu K, Qu L, Shimada SG, Nie H, and LaMotte RH (2014). Enhanced scratching elicited by a pruritogen and an algogen in a mouse model of contact hypersensitivity. Neurosci. Lett 579, 190–194. [PubMed: 24704378]

Galli SJ, and Tsai M (2012). IgE and mast cells in allergic disease. Nat. Med 18, 693–704. [PubMed: 22561833]

Gaudenzio N, Sibilano R, Marichal T, Starkl P, Reber LL, Cenac N, McNeil BD, Dong X, Hernandez JD, Sagi-Eisenberg R, et al. (2016). Different activation signals induce distinct mast cell degranulation strategies. J. Clin. Invest 126, 3981–3998. [PubMed: 27643442]

Gimenez-Rivera VA, Siebenhaar F, Zimmermann C, Siiskonen H, Metz M, and Maurer M (2016). Mast cells limit the exacerbation of chronic allergic contact dermatitis in response to repeated allergen exposure. J. Immunol 197, 4240–4246. [PubMed: 27807191]

Grimbaldeston MA, Nakae S, Kalesnikoff J, Tsai M, and Galli SJ (2007). Mast cell-derived interleukin 10 limits skin pathology in contact dermatitis and chronic irradiation with ultraviolet B. Nat. Immunol 8, 1095–1104. [PubMed: 17767162]

Han L, Ma C, Liu Q, Weng HJ, Cui Y, Tang Z, Kim Y, Nie H, Qu L, Patel KN, et al. (2013). A subpopulation of nociceptors specifically linked to itch. Nat. Neurosci 16, 174–182. [PubMed: 23263443]

Harvima IT, Nilsson G, and Naukkarinen A (2010). Role of mast cells and sensory nerves in skin inflammation. G. Ital. Dermatol. Venereol 145, 195–204. [PubMed: 20467393]

Kamo A, Negi O, Tengara S, Kamata Y, Noguchi A, Ogawa H, Tominaga M, and Takamori K (2014). Histamine H(4) receptor antagonists ineffective against itch and skin inflammation in atopic dermatitis mouse model. J. Invest. Dermatol 134, 546–548. [PubMed: 23962807]

Kamohara M, Matsuo A, Takasaki J, Kohda M, Matsumoto M, Matsumoto S, Soga T, Hiyama H, Kobori M, and Katou M (2005). Identification of MrgX2 as a human G-protein-coupled receptor for proadrenomedullin N-terminal peptides. Biochem. Biophys. Res. Commun 330, 1146–1152. [PubMed: 15823563]

Kapas S, Tenchini ML, and Farthing PM (2001). Regulation of adrenomedullin secretion in cultured human skin and oral keratinocytes. J. Invest. Dermatol 117, 353–359. [PubMed: 11511315]

Katagiri K, Arakawa S, Hatano Y, and Fujiwara S (2006). Fexofenadine, an H1-receptor antagonist, partially but rapidly inhibits the itch of contact derma titis induced by diphenylcyclopropenone in patients with alopecia areata. J. Dermatol 33, 75–79. [PubMed: 16556272]

Kim YS, Anderson M, Park K, Zheng Q, Agarwal A, Gong C, Saijilafu Young, L., He S, LaVinka PC, et al. (2016). Coupled activation of primary sensory neurons contributes to chronic pain. Neuron 91, 1085–1096. [PubMed: 27568517]

Kim YS, Chu Y, Han L, Li M, Li Z, LaVinka PC, Sun S, Tang Z, Park K, Caterina MJ, et al. (2014). Central terminal sensitization of TRPV1 by descending serotonergic facilitation modulates chronic pain. Neuron 81, 873–887. [PubMed: 24462040]

Kleij HP, and Bienenstock J (2005). Significance of conversation between mast cells and nerves. Allergy Asthma Clin. Immunol 1, 65–80. [PubMed: 20529227]

Kostner L, Anzengruber F, Guillod C, Recher M, Schmid-Grendelmeier P, and Navarini AA (2017). Allergic contact dermatitis. Immunol. Allergy Clin. North Am. 37, 141–152. [PubMed: 27886903]

Kuwasako K, Kitamura K, Ishiyama Y, Washimine H, Kato J, Kangawa K, and Eto T (1997). Purification and characterization of PAMP-12 (PAMP [9–20]) in porcine adrenal medulla as a major endogenous biologically active peptide. FEBS Lett. 414, 105–110. [PubMed: 9305741]

Li M, Hener P, Zhang Z, Kato S, Metzger D, and Chambon P (2006). Topical vitamin D3 and low-calcemic analogs induce thymic stromal lymphopoietin in mouse keratinocytes and trigger an atopic dermatitis. Proc. Natl. Acad. Sci. USA 103, 11736–11741. [PubMed: 16880407]

Liu B, Tai Y, Achanta S, Kaelberer MM, Caceres AI, Shao X, Fang J, and Jordt SE (2016). IL-33/ST2 signaling excites sensory neurons and mediates itch response in a mouse model of poison ivy contact allergy. Proc. Natl. Acad. Sci. USA 113, E7572–E7579. [PubMed: 27821781]

Liu Q, Tang Z, Surdenikova L, Kim S, Patel KN, Kim A, Ru F, Guan Y, Weng HJ, Geng Y, et al. (2009). Sensory neuron-specific GPCR Mrgprs are itch receptors mediating chloroquine-induced pruritus. Cell 139, 1353–1365. [PubMed: 20004959]

Liu Q, Weng HJ, Patel KN, Tang Z, Bai H, Steinhoff M, and Dong X (2011). The distinct roles of two GPCRs, MrgprC11 and PAR2, in itch and hyperalgesia. Sci. Signal 4, ra45. [PubMed: 21775281]

McNeil BD, Pundir P, Meeker S, Han L, Undem BJ, Kulka M, and Dong X (2015). Identification of a mast-cell-specific receptor crucial for pseudo-allergic drug reactions. Nature 519, 237–241. [PubMed: 25517090]

Meixiong J, and Dong X (2017). Mas-related G protein-coupled receptors and the biology of itch sensation. Annu. Rev. Genet 51, 103–121. [PubMed: 29178819]

Metcalfe DD, Baram D, and Mekori YA (1997). Mast cells. Physiol. Rev 77, 1033–1079. [PubMed: 9354811]

Miyamoto T, Nojima H, Shinkado T, Nakahashi T, and Kuraishi Y (2002). Itch-associated response induced by experimental dry skin in mice. Jpn. J. Pharmacol 88, 285–292. [PubMed: 11949883]

Morita T, McClain SP, Batia LM, Pellegrino M, Wilson SR, Kienzler MA, Lyman K, Olsen AS, Wong JF, Stucky CL, et al. (2015). HTR7 mediates serotonergic acute and chronic itch. Neuron 87, 124–138. [PubMed: 26074006]

Motakis E, Guhl S, Ishizu Y, Itoh M, Kawaji H, de Hoon M, Lassmann T, Carninci P, Hayashizaki Y, Zuberbier T, et al.; FANTOM consortium (2014). Redefinition of the human mast cell transcriptome by deep-CAGE sequencing. Blood 123, e58–e67. [PubMed: 24671954]

Nattkemper LA, Tey HL, Valdes-Rodriguez R, Lee H, Mollanazar NK, Albornoz C, Sanders KM, and Yosipovitch G (2018). The genetics of chronic itch: gene expression in the skin of atopic dermatitis and psoriasis patients with severe itch. J. Invest. Dermatol 138, 1311–1317. [PubMed: 29317264]

Ng MF (2010). The role of mast cells in wound healing. Int. Wound J. 7, 55–61. [PubMed: 20409251]

Nothacker HP, Wang Z, Zeng H, Mahata SK, O'Connor DT, and Civelli O (2005). Proadrenomedullin N-terminal peptide and cortistatin activation of MrgX2 receptor is based on a common structural motif. Eur. J. Pharmacol 519, 191–193. [PubMed: 16111673]

Paton WD (1951). Compound 48/80: a potent histamine liberator. Br. J. Pharmacol. Chemother 6, 499–508. [PubMed: 14878986]

Peiser M, Tralau T, Heidler J, Api AM, Arts JH, Basketter DA, English J, Diepgen TL, Fuhlbrigge RC, Gaspari AA, et al. (2012). Allergic contact dermatitis: epidemiology, molecular mechanisms, in vitro methods and regulatory aspects. Current knowledge assembled at an international work shop at BfR, Germany. Cell. Mol. Life Sci. 69, 763–781. [PubMed: 21997384]

Reddy AT, Lakshmi SP, and Reddy RC (2012). Murine model of allergen induced asthma. J. Vis. Exp 63, e3771.

Robas N, Mead E, and Fidock M (2003). MrgX2 is a high potency cortistatin receptor expressed in dorsal root ganglion. J. Biol. Chem 278, 44400–44404. [PubMed: 12915402]

Scholzen TE, Steinhoff M, Bonaccorsi P, Klein R, Amadesi S, Geppetti P, Lu B, Gerard NP, Olerud JE, Luger TA, et al. (2001). Neutral endopeptidase terminates substance P-induced inflammation in allergic contact dermatitis. J. Immunol 166, 1285–1291. [PubMed: 11145711]

Shim WS, and Oh U (2008). Histamine-induced itch and its relationship with pain. Mol. Pain 4, 29. [PubMed: 18667087]

Shimada SG, Shimada KA, and Collins JG (2006). Scratching behavior in mice induced by the proteinase-activated receptor-2 agonist, SLIGRL-NH2. Eur. J. Pharmacol 530, 281–283. [PubMed: 16356490]

Subramanian H, Gupta K, Guo Q, Price R, and Ali H (2011). Mas-related gene X2 (MrgX2) is a novel G protein-coupled receptor for the antimicrobial peptide LL-37 in human mast cells: resistance to receptor phosphorylation, desensitization, and internalization. J. Biol. Chem 286, 44739–44749. [PubMed: 22069323]

Takamori A, Nambu A, Sato K, Yamaguchi S, Matsuda K, Numata T, Sugawara T, Yoshizaki T, Arae K, Morita H, et al. (2018). IL-31 is crucial for induction of pruritus, but not inflammation, in contact hypersensitivity. Sci. Rep 8, 6639. [PubMed: 29703903]

Usatine RP, and Riojas M (2010). Diagnosis and management of contact dermatitis. Am. Fam. Physician 82, 249–255. [PubMed: 20672788]

Usoskin D, Furlan A, Islam S, Abdo H, Lönnerberg P, Lou D, Hjerling-Leffler J, Haeggström J, Kharchenko O, Kharchenko PV, et al. (2015). Unbiased classification of sensory neuron types by large-scale single-cell RNA sequencing. Nat. Neurosci 18, 145–153. [PubMed: 25420068]

van Diest SA, Stanisor OI, Boeckxstaens GE, de Jonge WJ, and van den Wijngaard RM (2012). Relevance of mast cell-nerve interactions in intestinal nociception. Biochim. Biophys. Acta 1822, 74–84. [PubMed: 21496484]

Wernersson S, and Pejler G (2014). Mast cell secretory granules: armed for battle. Nat. Rev. Immunol 14, 478–494. [PubMed: 24903914]

Yamaguchi T, Nagasawa T, Satoh M, and Kuraishi Y (1999). Itch-associated response induced by intradermal serotonin through 5-HT2 receptors in mice. Neurosci. Res 35, 77–83. [PubMed: 10616911]

Highlights

- Mrgprb2 is a mast cell (MC)-specific receptor that mediates non-histaminergic itch

- Compared to FcεRI, Mrgprb2 activation releases more tryptase and less monoamines

- Mrgprb2 activation of MCs excites non-histaminergic itch-sensory neurons

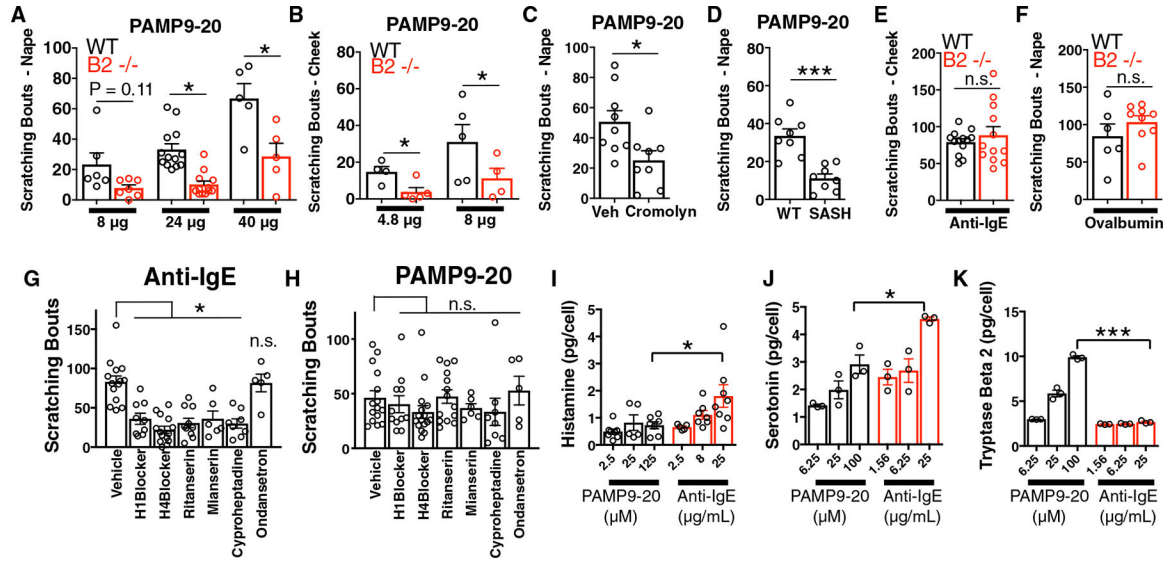- MRGPRX2 may be a target for allergic contact dermatitis-associated itch in humans

Figure 1. Compared with FcεRI Activation, Mrgprb2 Agonist PAMP9–20 Elicits Non-histaminergic Itch and Differential Pruritogen Release

(A–H) Scratching bouts from injection of pruritogen at either the nape or the cheek (mean plus SEM depicted). Each open circle represents an independent mouse data point. *p < 0.05; ***p < 0.001; n.s., not significant by two-tailed unpaired Student's t test. (A and B) PAMP9–20 injection into either the nape (50 μL) (A) or cheek (10 μL) (B) of WT and *Mrgprb2*^{−/−} (B2 −/−) animals. (A) 8 μg: WT, n = 6; B2 −/−, n = 7; 24 μg: WT, n = 13, B2 −/−, n = 12; 40 μg: WT, n = 5, B2 −/−, n = 5. (B) 4.8 μg: WT, n = 4, B2 −/−, n = 4; 8 μg: WT, n = 5, B2 −/−, n = 4. (C) Injection of 24 μg PAMP9–20 (50 μL of 300 μM) at the nape in the presence of either vehicle (Veh) or cromolyn. Vehicle, n = 9; cromolyn n = 8. (D) Injection of 24 μg PAMP9–20 (50 μL of 300 μM) into the nape of WT and SASH (cKit[W-sh]) mice. For both, n = 8. (E) 1 μg anti-IgE injection into WT and B2 −/− mice. WT, n = 7; B2 −/−, n = 6. (F) 50 μg ovalbumin injection into sensitized WT and B2 −/− animals. WT, n = 6; B2 −/−, n = 9. (G) 1 μg anti-IgE injection at the cheek with the indicated antagonist. Vehicle, n = 13; H1 blocker, n = 9; H4 blocker, n = 14; ritanserin, n = 10; mianserin, n = 6; cyproheptadine, n = 8; ondansetron, n = 5. (H) 24 μg PAMP9–20 injection at the nape with the indicated antagonist. Vehicle, n = 15; H1 blocker, n = 11; H4 blocker, n = 16; ritanserin, n = 14; mianserin, n = 6; cyproheptadine, n = 8; ondansetron, n = 5.

(I–K) *In vitro* release of histamine (I), serotonin (J), and tryptase beta 2 (K) from mouse peritoneal mast cells upon stimulation by various concentrations of either PAMP9–20 or anti-IgE. Open circles depict independent biological replicates from peritoneal mast cells isolated from >4 animals (mean plus SEM depicted). *p < 0.05; ***p < 0.001 by two-tailed unpaired Student's t test. (I) PAMP9–20: 2.5, n = 8; 25, n = 5; 125, n = 7. For anti-IgE: 2.5, n = 5; 8, n = 7; 25, n = 8. (J and K) All concentrations n = 3.
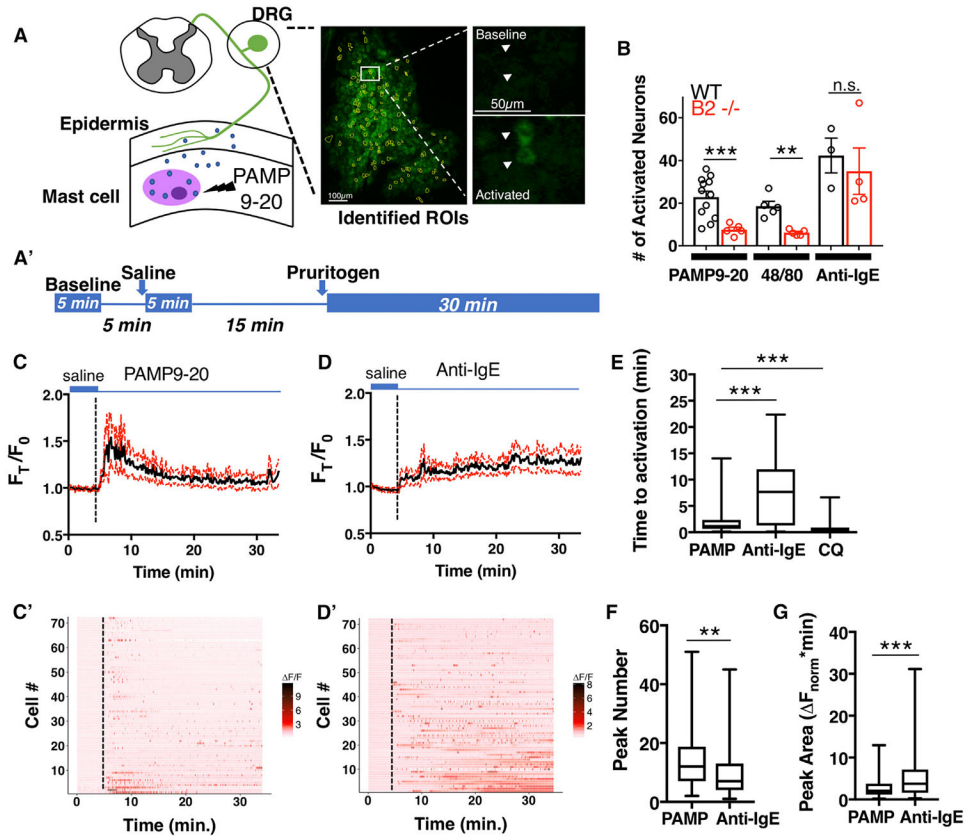
See also Figures S1 and S2.

Figure 2. Differential Mast Cell Agonism Exhibits Varied Sensory Neuron Activation Profiles

(A and A′) Graphical depiction (A) and experimental flowchart (A′) of *in vivo* Ca^{2+} imaging of Pirt-Cre-GCaMP6s sensory neurons. White arrowheads indicate activated neurons.

(B) Total number of activated neurons for the labeled compound (mean plus SEM depicted). Open circles represent imaging trials from independent mice. **$p < 0.01$; ***$p < 0.001$; n.s., not significant by two-tailed unpaired Student's t test. PAMP9–20: WT, n = 12, B2 −/−, n = 5; compound 48/80: WT, n = 5, B2 −/−, n = 5; anti-IgE: WT, n = 3, B2 −/−, n = 4.

(C, D, C′, and D′) Averaged Ca^{2+} imaging traces with ±95% confidence intervals (CIs) (C and D) and heatmaps (C′ and D′) of individual neurons activated by 300 mM PAMP9–20 (C and C′; n = 72) and 100 μg/mL anti-IgE (D and D′; n = 72).<p/>(E–G) Box (25th and 75th percentiles) and whisker (max and min) plots. **$p < 0.01$; ***$p < 0.001$ by two-tailed unpaired Student's t test. (E) Time to first detected activation within trial period for neurons activated by the indicated test compounds. PAMP9–20, n = 95; CQ, n = 79; anti-IgE, n = 79.

(F) Number of Ca^{2+} signal peaks (>20% increase over baseline) within imaging trial period. PAMP9–20, n = 74; anti-IgE, n = 85. (G) Positive peak area (amplitude over baseline 3 duration) within the imaging trial period. PAMP9–20, n = 74; anti-IgE, n = 85.
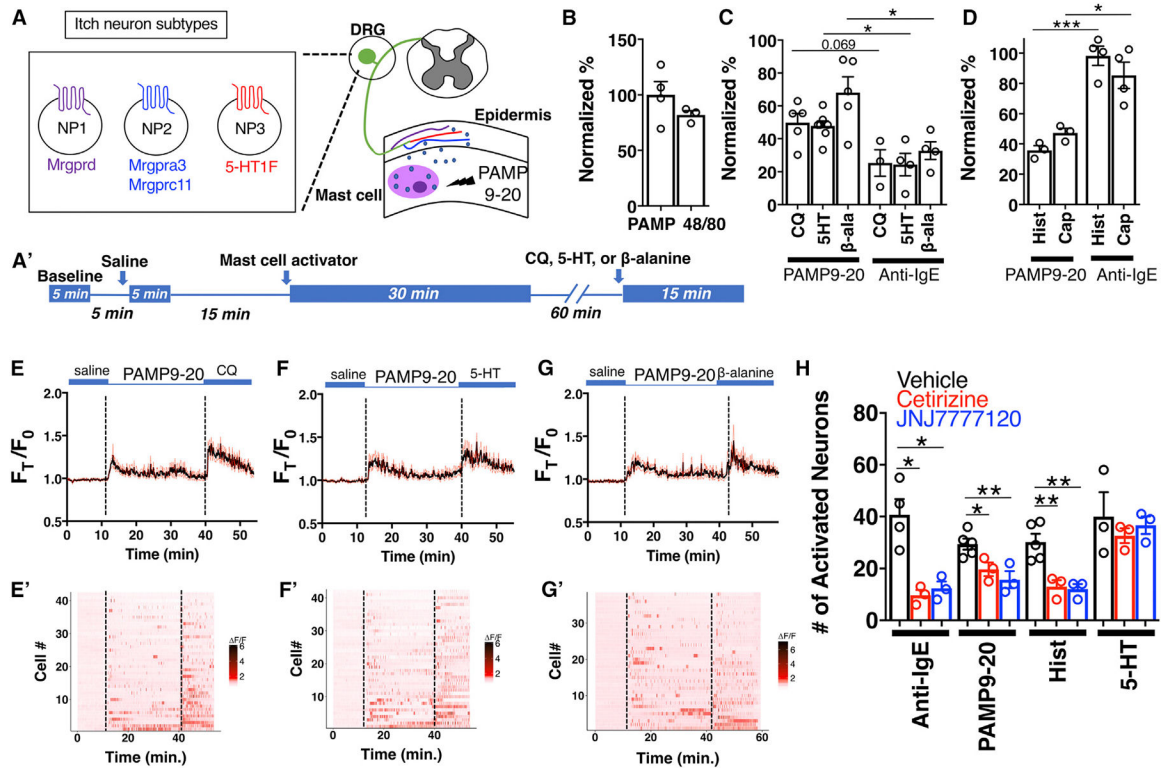
See also Figure S3.

Figure 3. Mrgprb2 Agonism Excites Multiple Itch Sensory Neuron Subtypes in an Activation Pattern Distinct from FcεRI

(A) Graphical depiction of itch neuron subtypes.

(A′) Experimental flowchart for *in vivo* Ca^{2+} imaging of mast cell agonists plus neuronal activators.

(B) Percent overlap of activated sensory neurons from a peripheral injection of 300 mM PAMP9–20 and a repeat injection of either 300 μM PAMP9–20 (n = 4) or 10 μg/mL compound 48/80 (n = 3). The percentages for these and subsequent data were normalized to repeated PAMP 9–20 injection.

(C) Normalized percentage overlap between 300 μM PAMP9–20 and 10 mM chloroquine (CQ; n = 5), 1 mM 5-HT (n = 6), or 10 mM β-alanine (n = 5) and between anti-IgE and CQ (n = 3), 5-HT (n = 4), or β-alanine (n = 4).

(D) Normalized percentage overlap between PAMP9–20 and either 9 mM histamine (n = 3) or 3 mM capsaicin (n = 3) and between anti-IgE and either histamine (n = 4) or capsaicin (n = 4).

(E–G and E′–G′) Averaged Ca^{2+} imaging traces with ±95% CIs (E–G) and heatmaps (E′–G′) of individual neurons activated by both PAMP9–20 and CQ (n = 42; E and E′), 5-HT (n = 42; F and F′), or β-alanine (n = 38; G and G′).

(H) Total number of neurons activated by the indicated test compound in the presence of vehicle, cetirizine (H1R antagonist), or JNJ7777120 (H4R antagonist). For anti-IgE: vehicle (veh), n = 4; cetirizine, n = 3; JNJ7777120, n = 3. For PAMP9–20: vehicle, n = 5; cetirizine, n = 3; JNJ7777120, n = 3. For histamine (Hist): vehicle, n = 5; cetirizine, n = 3; JNJ7777120, n = 3. For 5-HT: vehicle, n = 3; cetirizine, n = 3; JNJ7777120, n = 3.

(C–H) Mean plus SEM is depicted. Open circles represent individual, imaged mouse DRGs. *p < 0.05; **p < 0.01; ***p < 0.001; n.s., not significant; two-tailed unpaired Student's t test.
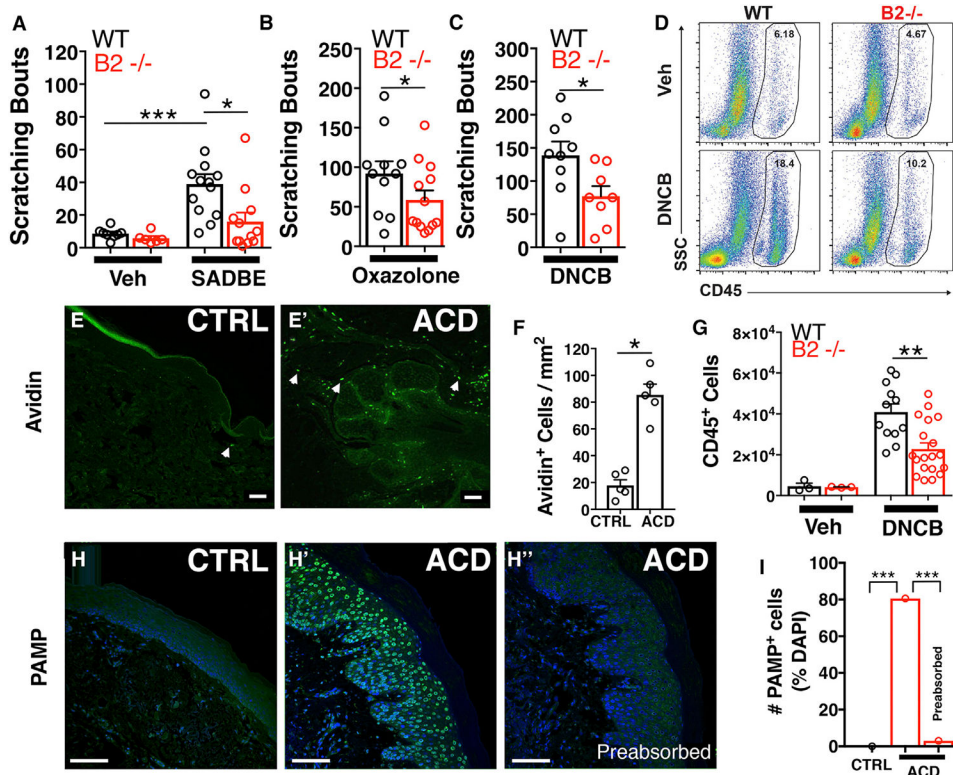
See also Figure S3.

Figure 4. Mast Cell Mrgprs Mediate a Component of Murine ACD Itch, and PAMP1–20, an MRGPRX2 Agonist, Is Upregulated in Human ACD Skin

(A–C) Scratching bouts in WT and *Mrgprb2*$^{-/-}$ animals with ACD (mean plus SEM depicted). Open circles represent independent mice. *p < 0.05; ***p < 0.001 by two-tailed unpaired Student's t test. For all compounds, vehicle was acetone: olive oil (4:1 v/v). (A) ACD elicited by squaric acid dibutyl ester (SADBE). Vehicle: WT, n = 8, B2 –/–, n = 6; SADBE: WT, n = 13, B2 –/–, n = 12. (B) 2-Phenyl-5-oxazolone (oxazolone). WT, n = 11, B2 –/–, n = 13. (C) 1-Chloro-2,4-dinitrobenzene (DNCB): WT, n = 9, B2 –/–, n = 8.

(D) Representative flow cytometry plots of DNCB-treated ear skin and vehicle treated ear skin from WT and B2 –/– animals. Numbers indicate the percentage of cells within boxes.

(E and E′) Representative images of control (E) and ACD (E′) human skin stained with avidin-fluorescein isothiocyanate (FITC). White arrows indicate positive staining. Scale bar, 100 μM.

(F) Number of avidin-stained cells per square millimeter (mean plus SEM depicted). Open circles represent separate sections. *p < 0.05 by two-tailed unpaired Student's t test. Control (CTRL), n = 5; contact dermatitis, n = 5.

(G) Number of CD45$^+$ leukocytes per biopsy from DNCB- and vehicle-treated WT and B2 –/– mouse ear skin (mean plus SEM depicted). Open circles represent independent samples from separate mice. **p < 0.01 by two-tailed unpaired Student's t test. For vehicle: WT, n = 3, B2 –/–, n = 3. For DNCB: WT, n = 12, B2 –/–, n = 19.

(H–H″) Representative images of control (H) and ACD human skin (H′ and H″) stained with either anti-PAMP (1–20) (human) antiserum (H and H′) or antiserum preabsorbed with excess PAMP1–20 peptide (H″). H′ and H″ are from adjacent sections from the same patient.

(I) Number of PAMP1–20-positive cells as a percentage of DAPI. Control, 0/1,616; ACD, 1,669/2,071; ACD preabsorbed, 63/2,097. ***$p < 0.001$ by chi-square test. Samples from at least 5 different ACD patients were tested.

See also Figure S4.

KEY RESOURCES TABLE

REAGENT or RESOURCE	SOURCE	IDENTIFIER
Antibodies		
Anti-Mouse IgE	Abcam	Cat#ab19967; RRID: AB_771797
PE anti-mouse CD45	BioLegend	Cat#103105; RRID: AB_312970
Brilliant Violet 510 anti-mouse/human CD11b	BioLegend	Cat#101245; RRID: AB_2561390
PerCP/Cy5.5 anti-mouse CD117	BioLegend	Cat#105823; RRID: AB_2131598
FITC anti-mouse CD45	BioLegend	Cat#103108; RRID: AB_312973
IgE Monoclonal (23G3), FITC	eBioscience	Cat#11–5992–81; RRID: AB_465342
FceR1 alpha Monoclonal (MAR-1), FITC	eBioscience	Cat#11–5898–81; RRID: AB_465307
TruStain FcX (anti-mouse CD16/32)	BioLegend	Cat#101320; RRID: AB_1574975
Goat anti-Rabbit IgG Secondary, Alexa Fluor 488	Thermo Fisher	Cat#A-11008; RRID: AB_143165
Anti-PAMP1–20 (human)	Peninsula Labs	Cat#T-4134.0050; RRID: AB_519203
Biological Samples		
Patient skin samples, control and allergic contact dermatitis	Skin Biology and Diseases Resource-based Center at the University of Pennsylvania	https://dermatology.upenn.edu/sbdre/
Chemicals, Peptides, and Recombinant Proteins		
PAMP9–20 peptide	Genscript	Custom Synthesis
PAMP1–20 peptide	Anaspec	Cat#AS-65455
Compound 48/80	Sigma	Cat#C2313
Albumin from chicken egg white	Sigma	Cat#A5503
Aluminum hydroxide, reagent grade	Sigma	Cat#239186
Cetirizine Hydrochloride	Tocris	Cat#2577
JNJ7777120	Tocris	Cat#4021
Ritanserin	Sigma	Cat#R103
Mianserin	Selleck Chemicals	Cat#S1382
Ondansetron	Selleck Chemicals	Cat#S1390
Cyproheptadine	Sigma	Cat#C3280000
Cromolyn sodium	Sigma	Cat#C0399
4-Nitrophenyl N-acetyl-β-D-glucosaminide	Sigma	Cat#N9376
Recombinant Mouse SCF Protein	Peprotech	Cat#455-MC-010
Fluo-4 Am, Cell permeant	Thermo fisher	Cat#F14201
Avidin-Fluorescein conjugate	Sigma	Cat#189727
Isolectin GS-IB$_4$ Alexa Fluor 488 conjugate	Thermo Fisher	Cat#I21411
Chloroquine	Sigma	Cat#C6628
β-alanine	Sigma	Cat#146064
5-HT	Sigma	Cat#H9523
Histamine	Sigma	Cat#H7125
Capsaicin	Sigma	Cat#M2028
Squaric acid dibutyl ester	Acros Organics	Cat#133170050
2-Phenyl-5-oxazolone	Alfa Aesar	Cat#L00194

REAGENT or RESOURCE	SOURCE	IDENTIFIER
1-Chloro-2,4-dinitrobenzene	Acros Organics	Cat#160511000
Olive Oil	Sigma	Cat#O1514
Calcipotriol hydrate	Sigma	Cat#C4369
Dispase II	Sigma	Cat#D4693
Collagenase II	Thermo Fisher	Cat#17101015
Collagenase IV	Thermo Fisher	Cat#17104019
Critical Commercial Assays		
Zombie Aqua Fixable Viability Kit	Biolegend	Cat#423101
Histamine ELISA Kit	Enzo Lifesciences	Cat#ENZ-IT140–0001
Tryptase Beta 2 ELISA Kit	CusaBio	Cat#EL024128MO
Serotonin ELISA Kit	Enzo Lifesciences	Cat#ADI-900–175
Experimental Models: Organisms/Strains		
Mouse: Mrgprb2–/–; C57BL/6J Mrgprb2 knockout	This lab	N/A
Mouse: Mrgprb2-Cre; C57BL/6J Cre-recombinase under Mrgprb2 promoter	This lab	N/A
Mouse: tdTomato (tdT); B6; 129S6-Gt(ROSA) 26Sor$^{tm14(CAG-tdTomato)Hze}$/J	Jackson Labs	Jax: 007908
Mouse: GCaMP6s; C57BL/6J ROSA26-lox-stop-lox GCaMP6s	Bergles Lab at Hopkins	N/A
Mouse: Pirt-Cre; C57BL/6J Cre-recombinase under Pirt promoter	This lab	N/A
Mouse: SASH; B6.Cg-Kit^{W-sh}/HNihrJaeBsmJ	Jackson Labs	Jax: 030764
Oligonucleotides		
Primers targeting Mrgprb2: forward 5'-gtcacagaccagtttaacacttcc, rever 5'- cagccatagccaggttgagaa	This paper; McNeil et al., 2015	N/A